Effects of tire - pavement contact pressure distributions on the response of asphalt concrete pavements

Yue, Z. Q.; Svec, O. J.

Canadian Journal of Civil Engineering, 22, 5, pp. 849-860, 1995-10-01

Effects of tire - pavement contact pressure distributions on the response of asphalt concrete pavements

NRCC-38864

Yue, Z.Q.; Svec, O.J.

October 1995

A version of this document is published in / Une version de ce document se trouve dans:
Canadian Journal of Civil Engineering, 22, (5), pp. 849-860, October 01, 1995

Effects of tire–pavement contact pressure distributions on the response of asphalt concrete pavements

Zhong Qi Yue and Otto J. Svec

Abstract: The paper presents the development of a computer program VIEM for the elastic analysis of multilayered elastic pavements under the action of arbitrary tire–pavement contact pressure distributions. The techniques adapted in VIEM primarily involves the use of a two-dimensional numerical integration to integrate point load solutions over the distributed pressure after discretizing the contact area into a finite number of triangular or quadrilateral elements. Values of contact pressure are inputted at the node points of discretized area. Numerical verification of VIEM indicates that numerical solution of high accuracy can be efficiently calculated for the elastic response of multilayered asphalt pavements. As a result, the determination of displacements and stresses (strains) can be achieved using a personal computer. With the use of VIEM, a theoretical investigation is further performed to illustrate the effects of tire–pavement contact pressure distributions on the response of asphalt concrete pavements. An *in situ* measured tire–pavement contact pressure distribution is utilized in the investigation. The response of asphalt concrete pavements due to the action of this measured contact pressure distribution is examined and compared with that due to the action of a uniform and circular contact pressure distribution by taking into account the influences of moduli and thicknesses of structural layers. The results of this investigation confirm theoretically a general consensus that details of the contact pressure distribution affect stresses and strains near the surface of the pavement, whereas the response in the lower layers depends mainly on the overall load. In particular, the contact pressure distributions have a significant effect on the horizontal tensile strains at the bottom of thin asphalt concrete layer which control the fatigue failure of asphalt pavements.

Key words: tire–pavevment interaction, three-dimensional stress analysis, asphalt concrete pavements, numerical integration, multilayered elastic solids, point load solution.

Résumé : Cet article traite du développement du programme informatique VIEM pour l'analyse de chaussées élastiques multicouches soumises à une répartition arbitraire des pressions de contact pneu–chaussée. Les techniques incorporées au programme VIEM ont recours principalement à l'intégration numérique bidimensionnelle de solutions de charge ponctuelle après la discrétisation de la surface de contact en un nombre fini d'éléments triangulaires et quadrilatéraux. Les valeurs des pressions de contact sont saisies aux points de noeud la surface discrétisée. La vérification effectuée par VIEM indique qu'une solution numérique de grande précision peut être calculée efficacement pour la réponse élastique de chaussées d'asphalte multicouches. Conséquemment, il est possible de déterminer les déplacements et les contraintes (déformations) à l'aide d'un ordinateur personnel. Une analyse théorique a été effectuée pour illustrer les effets de la répartition des pressions de contact pneu–chaussée sur le comportement de chaussées en béton bitumineux à l'aide de VIEM. Une répartition mesurée sur le terrain a été utilisée dans cette analyse. La réponse des chaussées en béton bitumineux soumises à l'action de cette répartition est examinée et comparée à la réponse de chaussées soumises à une répartition des pressions de contact uniformes et circulaires, en tenant compte des influences des modules et des épaisseurs des couches constituantes. Les résultats de cette analyse confirment que des détails de la répartition des pressions de contact influent sur les contraintes et les déformations à proximité de la surface de la chaussée, alors que la réponse au niveau des couches inférieures dépend surtout de la charge globale. De manière plus précise, la répartition des pressions de contact a un effet

Received June 21, 1994. Revised manuscript accepted January 11, 1995.

Z.Q. Yue and O.J. Svec. Infrastructure Laboratory, Institute for Research in Construction, National Research Council Canada, Ottawa, ON K1A 0R6, Canada.

Written discussion of this paper is welcomed and will be received by the Editor until February 29, 1996 (address inside front cover).

Can. J. Civ. Eng. **22**: 849–860 (1995). Printed in Canada / Imprimé au Canada

important sur les déformations horizontales dues à la traction, dans la partie inférieure de la couche de béton bitumineux qui contrôle la défaillance des chaussées d'asphalte causée par la fatigue.

Mots clés : interaction pneu–chaussée, analyse tridimensionnelle des contraintes, chaussées en béton bitumineux, integration numérique, solides élastiques multicouches, solutions de charge ponctuelle.
[Traduit par la rédaction]

1. Introduction

A vehicle meets the pavement at the tire–pavement interface. Tire–pavement contact pressure is the interaction stress between the rolling tire and pavement over an imprint area at the tire–pavement interface due to the action of vehicle axle load. Conventional approach in structural design and analysis of asphalt concrete pavements assumes that the vertical component of the contact pressure is uniformly distributed over a circular imprint area and is nominally equal to the tire inflation pressure (Monismith 1992). The assumption of uniformly circular contact pressure distribution seems to be adequate for asphalt pavement design and simplifies considerably the theoretical relationships of pavement performance used by highway engineers. However, considerable experimental evidence exists to suggest that this assumption is not always valid (e.g., Marshek et al. 1986*a*; Tielking and Roberts 1987; de Beer 1994). For instance, field measurements by Huhtala and Pihlajamaki (1990) indicated that the highest contact pressure was in the middle of a tire–pavement contact area and could be 20%, 35%, and 60% higher than the tire inflation pressures at 1, 0.75, and 0.5 MPa, respectively. The measured truck tire–pavement contact pressures were nonuniformly distributed over noncircular imprint areas. Furthermore, the characteristics of tires used in vehicles have changed dramatically since the 1962 AASHO road test (Morris 1987). The AASHO road test developed the relationships between the traffic and pavement damage and formed the empirical basis of pavement design and truck regulation. The test vehicles predominantly used bias-ply tires to 0.55 MPa (80 psi) cold air inflation pressure at that time. At present, radial-ply tires predominate on heavy trucks, and tire inflation pressures of 0.69–0.76 MPa (100–110 psi) are typical. New tire designs, such as low profile tires and wide base single tires to replace the dual tires, are gaining acceptance. Such changes of tire characteristics have an impact on the pavement performance and complicate the study of effects of tire–pavement contact pressure on the pavement response.

A number of authors, including Christison et al. (1978), Marshek et al. (1986*a*, 1986*b*), Chen et al. (1986), Roberts (1987), Uzan and Sides (1987), Christison (1989), Krarup (1991), and Groenendijk et al. (1994), have measured or calculated the influences of tire–pavement contact pressure on the stresses and strains in asphalt concrete pavements. It is a general consensus that details of the contact pressure distributions affect stresses and strains near the surface of the pavements, whereas the response in the lower layers depends mainly on the overall load.

The objective of the present study is to further investigate the effects of tire–pavement contact pressure distribution on the response of asphalt concrete pavements using a new computer program VIEM. The computer program VIEM, developed at the Infrastructure Laboratory, is based on an analytical solution of a multilayered elastic solid subjected to a general surface traction (Yue 1995). A typical contact pressure distribution measured by Huhtala and Pihlajamaki (1990) is used in the investigation. This contact pressure distribution was measured between a truck tire and an asphalt concrete pavement at the truck speed of 50 km/h. The responses of asphalt concrete pavements due to the actions of either the measured contact pressure distribution or a uniform circular contact pressure distribution are calculated using the computer program VIEM with a PC 486 DX66. The results of the critical displacements and strains and stresses in the asphalt concrete pavements due to the two contact pressure distributions are presented and compared by taking into account the influences of structural layer moduli and thicknesses. The results presented in the paper show that the computer program VIEM can be applied to the calculation of pavement responses under actual contact pressure distributions and that the contact pressure distributions have a significant effect on the strains and stresses in the surface layer.

2. Theoretical background and computer program VIEM

Many computer programs such as BISAR, ELSYM, CHEV, PDMAP, VESYS, CHEVIT, and CIRCLY have been developed to calculate the responses of multilayered elastic pavement systems subjected to traffic loading (Monismith 1992). One of the main constraints associated with these well-known computer programs in pavement engineering is that the applied contact pressure has to be distributed over either one or more circular areas and the load distribution over each circular area has to be uniform. Consequently, these computer programs cannot be directly applied to the evaluation of pavement response when the tire–pavement contact pressure is nonuniformly distributed over a noncircular contact area.

For example, Marshek et al. (1986*b*) approximated a laboratory measured contact pressure to a nonuniform concentric circular pressure distribution and used the computer program BISAR in conjunction with superposition principle to calculate the asphalt pavement response. Later, Chen et al. (1986) re-evaluated the effects of contact pressure distribution on pavement response using a three-dimensional (3-D) finite element approach. A linear elastic, static, finite element program called TEXGAP-3D was used in the analysis in order to accommodate the nonuniform and noncircular contact pressure distribution measured statically from a laboratory test. This problem was further examined by Uzan and Sides (1987) using a numerical integration technique. The theoretical results of layered elastic systems given by Schiffman (1962) were utilized in the calculation of asphalt pavement response under a point load condition. The point load results were then used together with superposition principle

to numerically integrate the solution for the pavement response due to a nonuniform and noncircular contact pressure distribution. A 4 × 4 Gauss quadrature scheme was adopted in the calculation of the two-dimensional (2-D) integration. Accurate results could be obtained. Yet, one of the limitations, as stated in the paper (Uzan and Sides 1987), was that the solution may not converge in some cases of very thick layers. Tielking and Roberts (1987) and Roberts (1987) modified the finite element code ILLIPAVE developed by Duncan et al. (1968) to allow a nonuniform and noncircular pressure distribution to be calculated. The tire–pavement contact pressure was numerically evaluated from a static finite element tire model. One of the advantages of using ILLIPAVE was that the moduli of nonstabilized pavement layers could be modelled as stress-sensitive materials.

The above literature review reveals that there is a need to develop a simplified computational procedure to calculate stably and accurately the stresses and deformation in multilayered elastic pavements due to the action of nonuniform and noncircular contact pressure. As a result, a computer program VIEM has been developed for this purpose and can be used in a personal computer. The analytical solution given by Yue (1995) for the 3-D response of a multilayered elastic solid subjected to a concentrated point traction is used in the computational scheme. Verification given in the report (Yue 1995) shows that there is no problem in the numerical evaluation of the point load solution $G(x, y, z)$ with high accuracy and efficiency. In particular, the singularity of the point load solution in a multilayered elastic solid was expressed in exact closed-form (in terms of elementary functions). The solution $S(x, y, z)$ for the 3-D response of a multilayered elastic pavement subjected to an arbitrary tire–pavement contact pressure $p(x, y)$ can be expressed as follows in a Cartesian coordinate system (x, y, z) using the superposition principle.

$$[1] \quad S(x, y, z) = \int\int_A p(\xi, \eta) G(x - \xi, y - \eta, z)\, d\xi\, d\eta$$

where the 2-D integration limit A is the imprint area.

In order to numerically calculate the 2-D integral [1], a concept of discretization technique, similar to that used in finite element methods, is adopted (e.g., Sharma and Rao 1984; Bickford 1990). The imprint (contact) area is discretized into triangular and (or) quadrilateral elements. The solution $S(x, y, z)$ ([1]) is then equal to the summation of the integrals $I_k(x, y, z)$ over the discretized triangular or quadrilateral elements A_k $(k = 1, 2, \ldots, N)$.

$$[2] \quad S(x, y, z) = \sum_{k=1}^{N} I_k(x, y, z)$$

Two isoparametric elements, i.e., the six-node triangular element and the eight-node quadrilateral element, are used to numerically calculate the integrals $I_k(x, y, z)$ over the discretized triangular and quadrilateral elements, respectively. For example, the following formulae are applicable to an eight-node quadrilateral element.

$$[3] \quad I_k(x, y, z) = \int\int_{A_k} p(\xi, \eta) G(x - \xi, y - \eta, z)\, d\xi\, d\eta$$

$$= \int_{-1}^{1}\int_{-1}^{1} p(\xi(s, t), \eta(s, t)) \times G(x - \xi(s, t), y - \eta(s, t), z) \times |J(s, t)|\, ds\, dt$$

$$= \sum_{i=1}^{m}\sum_{j=1}^{n} p(\xi(s_i, t_j), \eta(s_i, t_j)) \times G(x - \xi(s_i, t_j), y - \eta(s_i, t_j), z) \times |J(s_i, t_j)| w_i w_j$$

where $|J(s, t)|$ is the determinant of the Jacobian matrix; s_i and t_j are the Gauss points; w_i and w_j are the Gauss weights; and m and n are the Gauss integration numbers for the local coordinates s and t, respectively. Similar formulae can be written for the case of a six-node triangular element (see, for example, Bickford 1990).

The following interpolation equations govern the relationship between the global coordinates (ξ, η) and the local coordinates (s, t).

$$\xi = \xi(s, t) = \sum_{l=1}^{L} \xi_l N_l(s, t)$$

[4]

$$\eta = \eta(s, t) = \sum_{l=1}^{L} \eta_l N_l(s, t)$$

where $L = 6$ or 8; (ξ_l, η_l) are the node coordinates in the global coordinate system; $N_l(s, t)$ $(l = 1, 2, \ldots, L)$ are the nondimensional interpolation functions of the six-node triangular or the eight-node quadrilateral elements and can be easily found in many finite element method textbooks (see, for example, Bickford 1990).

The applied contact pressure distribution $p(\xi, \eta)$ over a triangular or quadrilateral element can be approximated using the pressure values at the node points; i.e.,

$$[5] \quad p(\xi, \eta) = p(\xi(s, t), \eta(s, t)) \approx \sum_{l=1}^{L} p_l N_l(s, t)$$

where p_l $(l = 1, 2, \ldots, L)$ are the inputted pressure values at the node points.

It is noted that the point load solution $G(x, y, z)$ has the singularities of $1/R$ and $1/R^2$ as $R = \sqrt{x^2 + y^2 + z^2} \to 0$ for displacements and stresses, respectively. As a result, the 2-D integrals in [1] for displacements and stresses become improper integrals as the evaluation point (x, y, z) is very close to the tire–pavement contact area A at the surface of the pavement $(z = 0)$. Numerical errors could be induced to the results (in particular, of the stresses) if the numerical integrations described above are directly applied (Sharma and Rao 1984; Uzan and Sides 1987). Special techniques are required to overcome the problem of improper integrals. For example, the closed-form solution for the singular terms in the point load solution $G(x, y, z)$ as $0 \le z/h_1 < 1$ (where h_1 is the thickness of the first layer) given by Yue (1995) can be used to treat the numerical problem. One may analytically integrate the parts of the integrals [1]–[3] associated with the singular terms.

Fig. 1. Discretizations of a circular area using (*a*) 12, (*b*) 20, (*c*) 36, and (*d*) 88 elements.

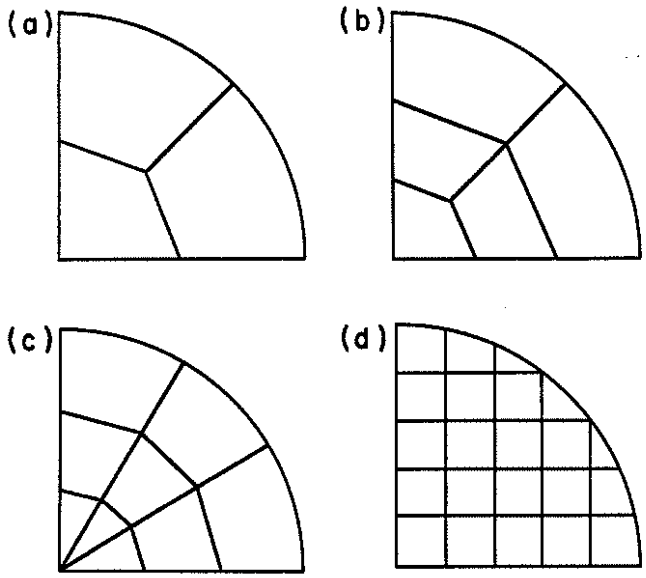

3. Numerical verification of VIEM

In the ensuing, a numerical example is given to verify the above discretization technique. In this example, the tire–pavement contact pressure is uniformly distributed over a circular area at the surface of a three-layered elastic pavement. The total applied load is 40 kN and the radius of the circular contact area is 150 mm. The moduli of the three layers (from top to bottom) are $E_1 = 3000$, $E_2 = 250$, and $E_3 = 50$ MPa. The Poisson ratios are $\nu_1 = 0.35$, $\nu_2 = 0.3$, and $\nu_3 = 0.4$. The thicknesses of the first and second layers are selected as $h_1 = 100$ and $h_2 = 250$ mm. The third layer, i.e., the subgrade is an elastic halfspace. The interface between any two connected layers is perfectly bonded. The circular imprint area is discretized into 12, 20, 36, or 88 elements with 3, 5, 9, or 22 elements in a quarter as shown in Fig. 1. The numerical results presented in this paper are only those for vertical displacements and radial normal strains in the pavement along the vertical axis ($r = 0$) and the radial axis ($z = 0$) using the integration order of 4×4.

Tables 1 and 2 illustrate the results of the vertical displacements along the vertical axis and the radial axis, respectively. Comparing with the exact solutions, the data presented in Tables 1 and 2 demonstrate that very accurate results can be achieved for displacements at any location of the multilayered elastic pavement using the discretization techniques. Increase in the discretization elements improves the accuracy of the numerical results for displacements. In particular, in the case of 88 elements, the relative errors between the exact solutions and the numerical results are less than 0.03% for the displacements at any point in the pavement. In the case of 12 elements, the relative errors are less than 0.2%.

The results of the radial normal strains are presented in Tables 3 and 4. These data in Tables 3 and 4 illustrate that increase in the discretization elements improves the accuracy of the numerical results for strains (or stresses) provided that the valuation point is not located within the tire–pavement contact area at the surface of the pavements. Yet if the evaluation point is located within the contact area, the increase in the discretization elements does not improve the accuracy of the numerical results for strains (or stresses). In particular, in the case of 88 elements, the relative errors between the exact and numerical solutions are 0.1% and 0.9% for the strains evaluated at the points ($z = 10$ mm, $r = 0$; or $z/a = 10/150 = 0.067$, $r = 0$) and ($z = 0$, $r = 155$ mm; or $z/a = 0$, $r/a = 155/150 = 1.033$), respectively. For the maximum tensile strain at the bottom of the asphalt concrete (AC) layer ($z = 100$ mm, $r = 0$), the relative errors between the exact and numerical solutions are less than 0.037% in the cases of 12 and 20 elements.

Table 1. Vertical displacements (mm) along the vertical axis where $r = 0$.

		Numerical solutions with the element number of			
z	Exact solution	12	20	36	88
0.0	0.71921	0.71834	0.71846	0.71724	0.71906
10.0	0.72115	0.72088	0.72069	0.72049	0.72114
15.0	0.72185	0.72141	0.72134	0.72166	0.72185
25.0	0.72277	0.72225	0.72226	0.72281	0.72277
50.0	0.72257	0.72206	0.72206	0.72248	0.72256
75.0	0.71912	0.71861	0.71861	0.71902	0.71912
100.0	0.71225	0.71174	0.71174	0.71215	0.71225
200.0	0.63719	0.63672	0.63672	0.63709	0.63719
350.0	0.56975	0.56932	0.56932	0.56966	0.56974

Table 2. Vertical displacements (mm) along the radial axis where $z = 0$.

		Numerical solutions with the element number of			
r	Exact solution	12	20	36	88
25.0	0.71694	0.71787	0.71521	0.71538	0.71639
50.0	0.71018	0.71138	0.70950	0.70951	0.71071
100.0	0.68390	0.68460	0.68308	0.68359	0.68444
150.0	0.64015	0.63933	0.63927	0.63984	0.64007
155.0	0.63426	0.63382	0.63381	0.63419	0.63426
160.0	0.62908	0.62862	0.62862	0.62899	0.62907
165.0	0.62413	0.62366	0.62366	0.62403	0.62413
175.0	0.61464	0.61416	0.61417	0.61454	0.61463
185.0	0.60547	0.60500	0.60501	0.60538	0.60547
200.0	0.59213	0.59167	0.59167	0.59204	0.59213
300.0	0.51233	0.51194	0.51194	0.51225	0.51233

The exact solutions of displacements and strains in Tables 1–4 are calculated using the following solution expression in a cylindrical coordinate system (Yue 1995) and were verified using the computer program ELSYM5.

$$[6] \quad S(r, z) = \frac{-P_z}{\pi a^2} \int_0^\infty \Phi(\rho, z/a) J_m(\rho r/a) J_1(\rho)\, d\rho$$

where P_z is the applied total load; a is the radius of a circular contact area; J_m is the Bessel function of the order m ($m = 0, 1, 2$); Φ are the analytical kernel functions of a multilayered elastic system (Yue 1995). The absolute and (or) relative errors of the semi-infinite integration are 10^{-6}

Table 3. Radial normal strains (10^{-3}) along the vertical axis where $r = 0$.

z	Exact solution	Numerical solutions with the element number of 12	20	36	88
0.0	−0.32423	−0.28591	−0.28591	−0.28601	−0.28603
10.0	−0.25415	−0.23848	−0.24353	−0.30327	−0.25394
15.0	−0.22100	−0.21039	−0.21981	−0.24993	−0.22137
20.0	−0.18895	−0.18591	−0.18931	−0.19878	−0.18902
25.0	−0.15788	−0.15768	−0.15810	−0.15828	−0.15788
30.0	−0.12766	−0.12805	−0.12770	−0.12510	−0.12766
50.0	−0.01276	−0.01278	−0.01273	−0.01178	−0.01276
75.0	0.12775	0.12773	0.12773	0.12783	0.12775
100.0	0.28163	0.28155	0.28155	0.28162	0.28163
200.0	0.24412	0.24398	0.24398	0.24409	0.24412
350.0	0.34854	0.34830	0.34830	0.34849	0.34854

Table 4. Radial normal strains (10^{-3}) along the radial axis where $z = 0$.

r	Exact solution	Numerical solutions with the element number of 12	20	36	88
25.0	−0.31883	−0.56934	−0.23884	−0.20631	−0.23799
50.0	−0.30273	−0.58382	−0.25607	−0.22706	−0.54917
100.0	−0.24142	−0.43818	−0.26538	−0.21836	−0.48787
150.0	−0.11899	−0.11905	−0.12346	−0.11994	−0.10040
155.0	−0.07474	−0.07787	−0.08044	−0.07384	−0.07406
160.0	−0.06858	−0.06693	−0.06747	−0.06724	−0.06862
165.0	−0.06240	−0.06107	−0.06118	−0.06197	−0.06241
175.0	−0.05011	−0.04977	−0.04978	−0.05011	−0.05011
185.0	−0.03823	−0.03814	−0.03814	−0.03823	−0.03823
200.0	−0.02170	−0.02166	−0.02166	−0.02169	−0.02170
300.0	0.03665	0.03664	0.03664	0.03665	0.03665

in calculation of the exact solutions.

In general, high accuracy and efficiency can be achieved for the numerical solutions using the discretization technique (VIEM). The accuracy of the numerical solutions increases rapidly as the distance of the evaluation location to the tire−pavement contact area increases. If it is necessary, special techniques should be adopted to accurately evaluate strains and stresses at the evaluation point located within the tire−pavement contact area at the surface of a multilayered pavement. Similar observations can be obtained for the numerical solutions using the integration order of 3 × 3. It is also noted that it requires about 7 s CPU time in a PC486 DX66 for VIEM to calculate the displacements and stresses and strains at a point (say, $r = 0$ and $z = 0$) using the 36 element discretization of the circular area with the Gauss integration order of 4 × 4 (the total Gauss points are 432). The remainder of this paper will be focused on the application of VIEM to evaluation of the pavement response under a measured tire−pavement contact pressure distribution.

4. A measured contact pressure distribution

Figure 2 illustrates a 3-D tire−pavement contact pressure distribution used in the analysis. This is an approximate simulation of the road measurement conducted by the Road and Traffic Laboratory, the Technical Research Centre of Finland (VTT) (Huhtala and Pihlajamaki 1990). The contact pressure was measured between the front tire of a truck and the pavement at the 50 km/h truck speed using a dynamic contact stress (pressure) measuring device. The axle load was 60 kN. The front tire was a bald radial tire and the cold air inflation pressure was 0.75 MPa. The contact pressure distribution is not symmetric. The tire imprint is longer on the right-hand side facing the traffic direction. The highest stress in the middle of the contact area is about 35% greater than the tire cold air inflation pressure. This measured contact pressure distribution is noted as MCP in the following analysis, for simplicity. For the purpose of comparison, the conventional tire−pavement contact pressure distribution (CCP), where the contact pressure is equal to the tire cold air inflation pressure (0.75 MPa) and is uniformly distributed over a circular area of 225.68 mm in diameter, is also employed. The total load for both contact pressure distributions (i.e., MCP and CCP) is 30 kN.

Typical three or four structural layers of asphalt pavements are selected for analyses. The mechanical properties of each structural layer are characterized by the effective elastic modulus E_j and the Poisson ratio ν_j, where the subscript j is the layer number. The thickness of each structural

Fig. 2. Distribution of a measured tire–pavement contact pressure and the Cartesian coordinates: (*a*) 3-D pressure distribution; (*b*) tire imprint area.

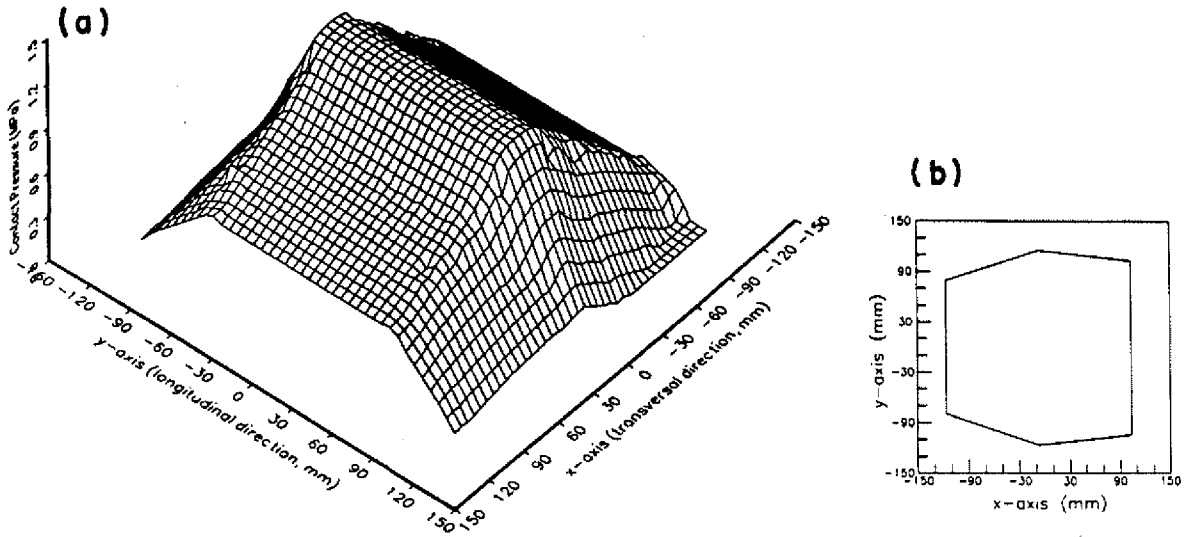

Fig. 3. 3-D response of a three-layer asphalt pavement induced by a measured tire–pavement contact pressure (MCP): (*a*) surface deflection contour (mm); (*b*) major horizontal strain contour at the bottom of asphalt concrete layer ($\times 10^{-4}$).

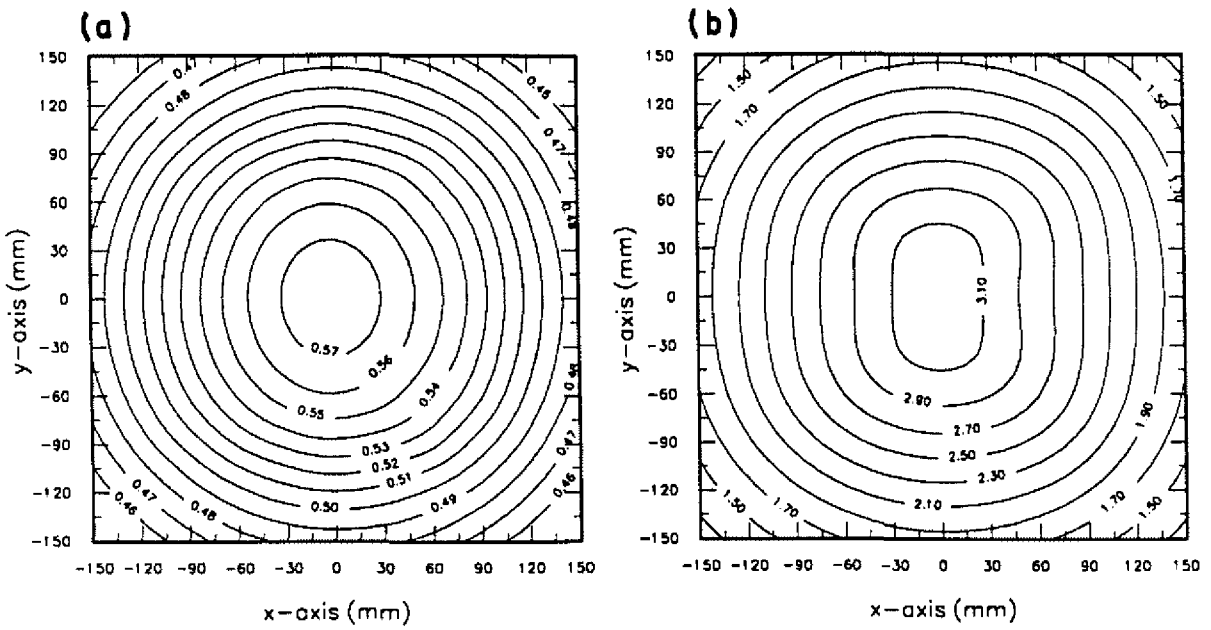

layer is noted as h_j. For a three-layer system, the asphalt concrete (AC), base, and subgrade layers are noted by j = 1, 2, and 3, respectively. For a four-layer system, the AC, base, subbase, and subgrade layers are noted by j = 1, 2, 3, and 4, respectively. An elastic halfspace representation is assumed for the subgrade. The interface between any two connected layers is assumed to be perfectly bonded.

A Cartesian coordinate system is used in the analysis (Fig. 2). The x and y axes are parallel to the transverse and longitudinal directions of the pavement respectively, while the z-axis represented pavement depth. The positive direction of the y-axis is the traffic direction. The origin of the Cartesian coordinates is located exactly at the loading centre of the experimentally measured contact pressure distribution.

5. 3-D response of an asphalt concrete pavement

Numerical results presented below illustrate the 3-D response of a typical three-layer asphalt pavement subjected to the measured tire–pavement contact pressure distribution (MCP). The material property and the thickness of each layer are selected as the same of those in the verification example of Sect. 3.

Figure 3*a* shows the contour of the vertical deflections at the surface of the pavement and Fig. 3*b* shows the contour of the major horizontal strains at the bottom of AC layer. These two figures illustrate that the nonaxisymmetric response of the asphalt pavement is mainly in the local region near the

Fig. 4. Response of a three-layer pavement subjected to a measured tire–pavement contact pressure distribution (MCP) or a conventional tire–pavement contact pressure distribution (CCP): (*a*) surface deflections; (*b*) major horizontal strains at the bottom of asphalt concrete (AC) layer.

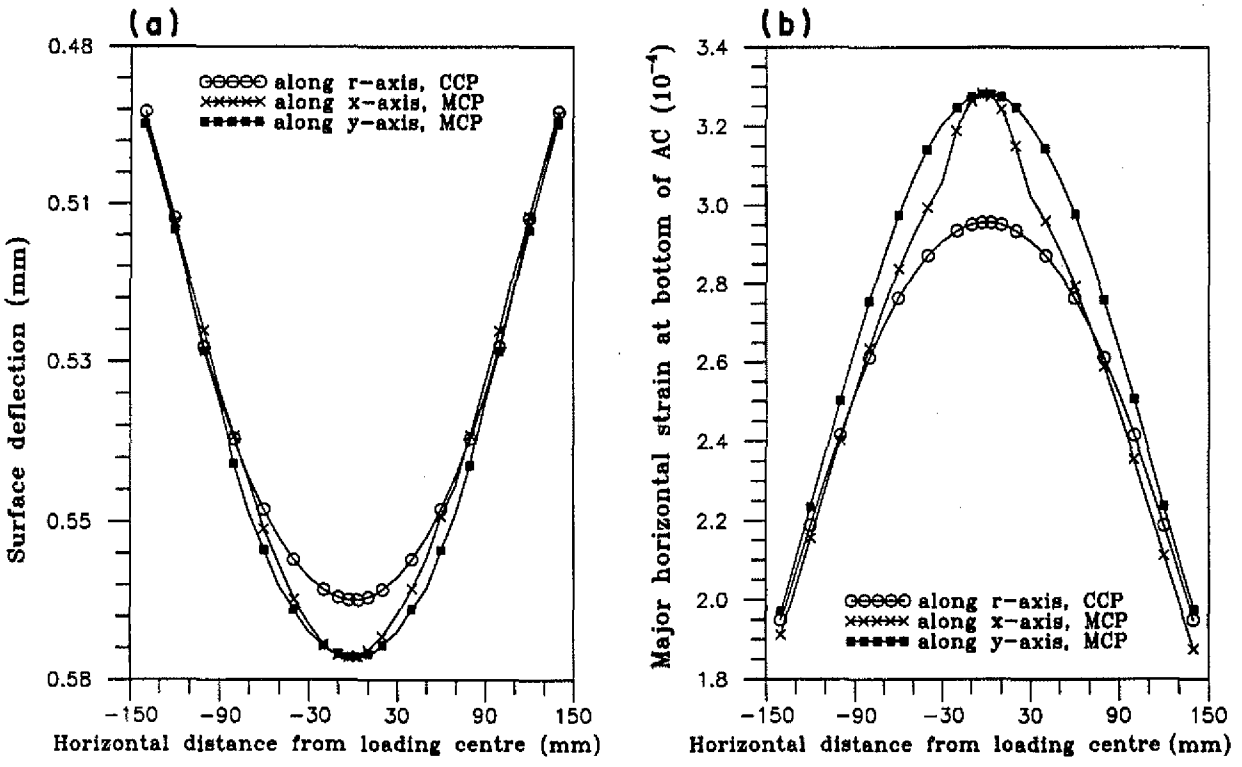

tire–pavement contact area. The minor and major axes of the 3-D response are along the transversal and longitudinal directions of the pavement, i.e., x and y axes, respectively. The maximum deflection and strain are located at the loading centre, which can be respectively observed in Figs. 4*a* and 4*b*.

For the purpose of comparison, the surface deflections and the major horizontal strains at the bottom of AC layer of the pavement induced by the uniform circular contact pressure distribution (CCP) are also plotted in Figs. 4*a* and 4*b*, respectively. The maximum differences between the pavement responses induced by the two contact pressure distributions (MCP and CCP) are located at the loading centre. The maximum surface deflection, the maximum tensile strain at the bottom of AC layer, and the maximum compressive strain at the top of subgrade layer induced by MCP increase respectively by 1.6%, 11%, and 0.5% over those induced by CCP.

6. Sensitivity analysis of pavement responses

With the use of the computer program VIEM, sensitivity analyses are carried out to illustrate the effect of tire–pavement contact pressure distributions on pavement responses. At first, a sensitivity analysis of a three-layer pavement system is performed. The considered variables are the layer thicknesses h_1 and h_2 and the layer moduli E_1, E_2, and E_3. The Poisson ratios (ν_1, ν_2, and ν_3) for the three structural layers are assigned to be 0.35, 0.3, and 0.4 respectively for this first example. The sensitivity analysis is focused on the effect of the two contact pressure distributions (i.e., MCP and CCP) on the maximum tensile strain ε_t at the bottom of AC layer and the maximum compressive strain ε_c at the top of subgrade.

The effects of the structural layer thicknesses (h_1 and h_2) on the pavement responses due to the MCP and the CCP are illustrated in Figs. 5–9. In these figures, the elastic moduli of the three layers (E_1, E_2, and E_3) are fixed to be 3000, 250, and 50 MPa, respectively. Figure 5 illustrates the variations of the maximum tensile strain ε_t at the bottom of AC layer due to the MCP and the CCP versus the thickness of AC layer (h_1). Two base layer thicknesses (h_2) of 100 and 400 mm are considered. There is a so-called critical thickness of h_1 (about 40–50 mm) at which ε_t is a maximum. Below this critical thickness, the thinner the AC layer, the smaller the value of ε_t. At $h_1 = 25$ mm, the percentage increases of ε_t due to the MCP over that due to the CCP are the largest ones which are equal to 82.9% and 112.6% for $h_2 = 100$ and 400 mm, respectively. With the increase of h_1 from 25 to 200 mm, the increases of ε_t due to the MCP over that due to the CCP are decreasing. At the critical thickness, the percentage increases are 33.0% and 43.6% for $h_2 = 100$ and 400 mm, respectively. At $h_1 = 200$ mm, the percentage increases are 2.64% and 3.19% for $h_2 = 100$ and 400 mm, respectively.

The effect of the base layer thickness (h_2) on the maximum tensile strain ε_t at the bottom of AC layer is presented in Fig. 6, where three AC layer thicknesses (h_1) of 50, 100, and 150 mm are used. With the increase of h_2 from 50 to 400 mm, the percentage increases of ε_t due to the MCP over that due to the CCP are slowly increasing. At $h_2 = 50$ mm,

Fig. 5. Maximum tensile strain at bottom of AC layer vs. AC layer thickness.

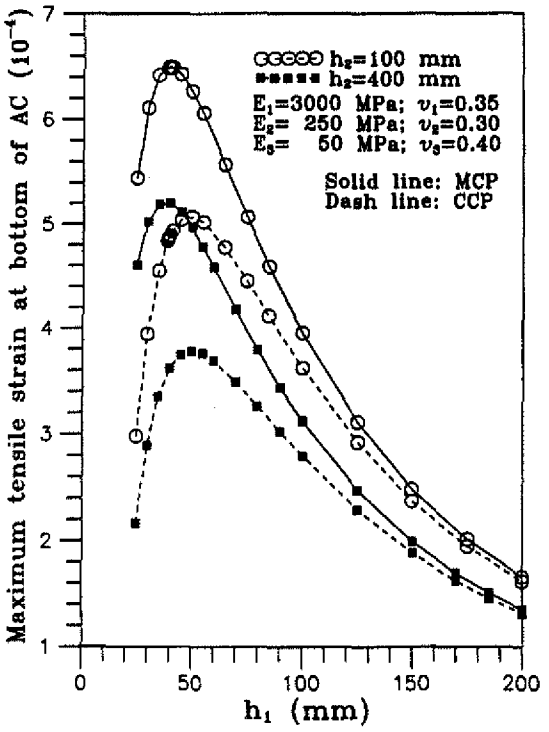

Fig. 6. Maximum tensile strain at bottom of AC layer vs. base layer thickness.

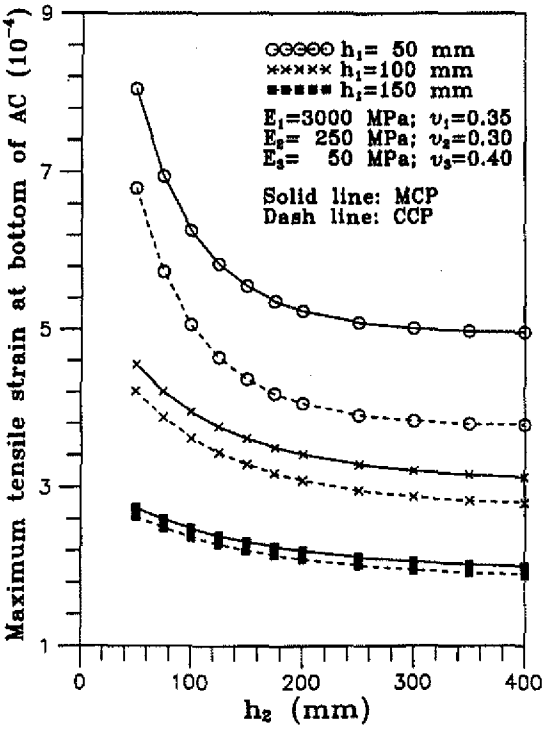

the percentage increases are 18.4%, 8.0%, and 4.2% for h_1 = 50, 100, and 150 mm, respectively. At h_2 = 400 mm, the percentage increases are 31.2%, 11.6%, and 5.7% for h_1 = 50, 100, and 150 mm, respectively.

Figure 7 illustrates the variations of the maximum compressive strain ε_c at the top of subgrade due to the MCP and the CCP versus the thickness of AC layer (h_1). Two base layer thicknesses (h_2) of 100 and 400 mm are considered. The increases of ε_c due to the MCP over that due to the CCP

Fig. 7. Maximum compressive strain at top of subgrade vs. AC layer thickness.

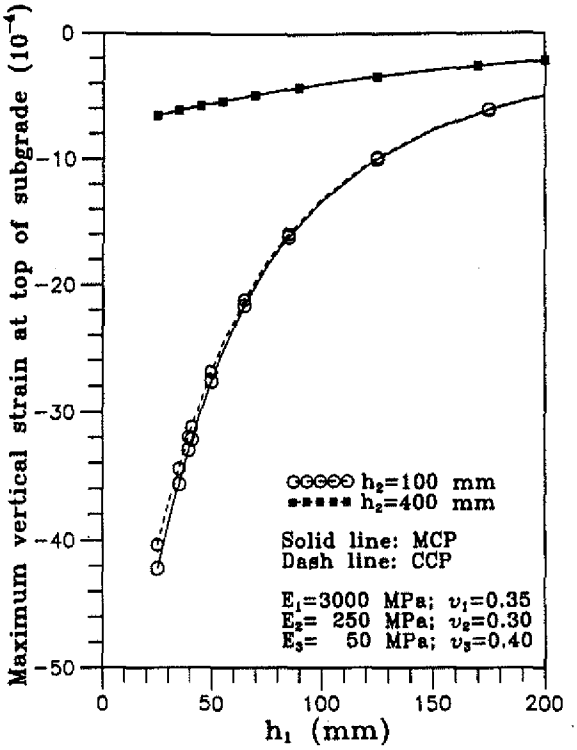

Fig. 8. Maximum compressive strain at top of subgrade vs. base layer thickness.

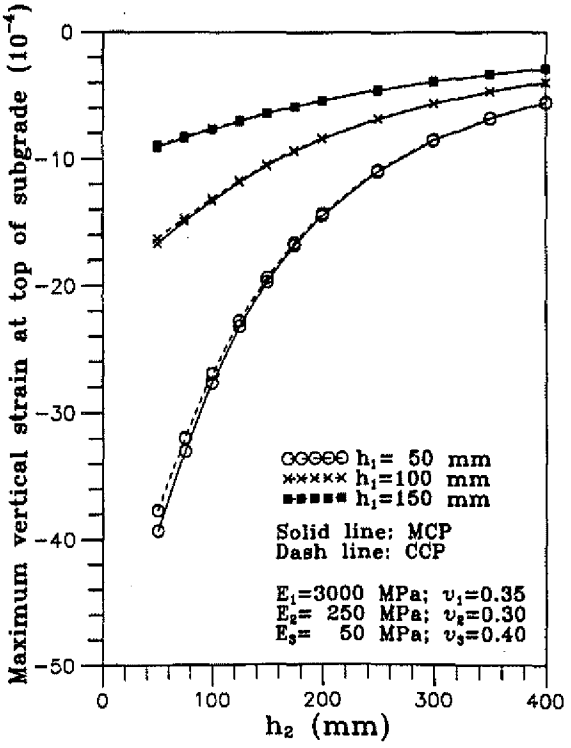

Fig. 9. Maximum tensile strain in asphalt pavement vs. AC layer thickness.

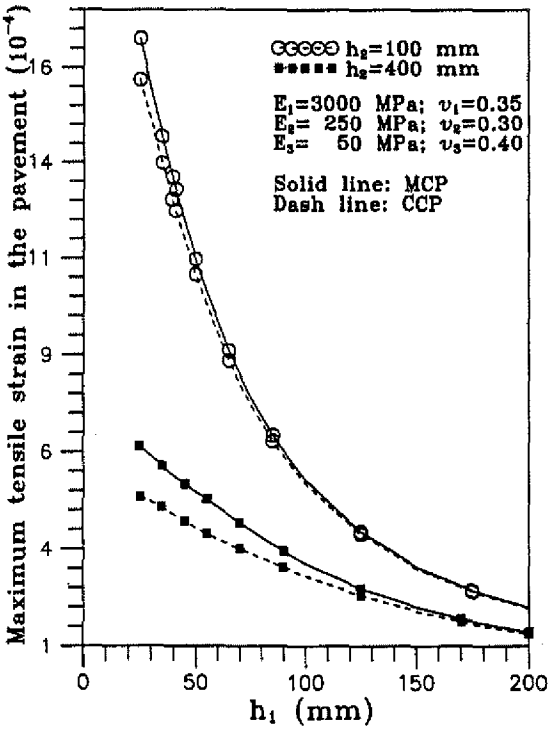

Fig. 10. Maximum tensile strain at bottom of AC layer vs. AC layer modulus.

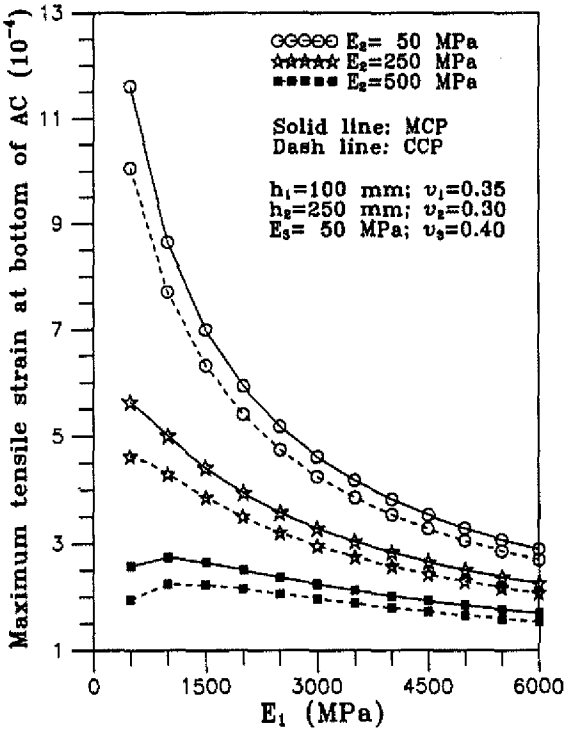

are very small and slowly decreasing with the increase of h_1 from 25 to 200 mm. At h_1 = 25 mm, the percentage increases are 4.5% and 0.55% for h_2 = 100 and 400 mm, respectively. At h_1 = 200 mm, the percentage increases are 0.64% and 0.16% for h_2 = 100 and 400 mm, respectively.

The effect of the base layer thickness (h_2) on the maximum compressive strain ε_c at the top of subgrade is presented in Fig. 8, where three AC layer thicknesses (h_1) of 50, 100, and 150 mm are used. The increases of ε_c due to the MCP over that due to the CCP are very small and slowly decreasing with the increase of h_2 from 50 to 400 mm. At h_2 = 50 mm, the percentage increases are 4.3%, 2.3%, and 1.4% for h_1 = 50, 100, and 150 mm, respectively. At h_2 = 400 mm, the percentage increases are 0.42%, 0.28%, and 0.19% for h_1 = 50, 100, and 150 mm, respectively.

It is noted herewith that the maximum horizontal tensile strains (ε_{tmax}) in the pavement may not locate at the bottom of AC layer when AC layer and (or) base layer are thin. Figure 9 illustrates the variations of ε_{tmax} versus the AC layer thickness (h_1), where the results of two base layer thicknesses of 100 and 400 mm are plotted. It is observed that (*i*) for h_2 = 100 mm, ε_{tmax} is located at different depths within the base layer and (*ii*) for h_2 = 400 mm, ε_{tmax} is located at different depths within the base layer when h_1 is less than about 70 mm and is located at the bottom of AC layer once h_1 is larger than about 70 mm. The maximum horizontal tensile strain ε_{tmax} is always increasing with the decrease in h_1 from 200 to 25 mm. The increases of ε_{tmax} due to the MCP over that due to the CCP are decreasing with the increase of h_1 from 25 to 200 mm. At h_1 = 50 mm, the percentage increases of ε_{tmax} due to the MCP over that due to the CCP are 6.88% and 26.96% for h_2 = 100 and 400 mm, respectively. At h_1 = 200 mm, the percentage increases are 0.99% and 3.19% for h_2 = 100 and 400 mm, respectively.

The effects of the structural layer moduli (E_1, E_2, and E_3) on the maximum tensile strain at the bottom of AC layer (ε_t) due to the actions of the MCP and the CCP are illustrated in Figs. 10–12. In these three figures, the thicknesses of the AC and base layers (h_1 and h_2) are fixed to be 100 and 250 mm, respectively. Figure 10 illustrates the variations of ε_t due to the MCP and the CCP versus E_1, where the base layer modulus (E_2) is 50, 250, or 500 MPa and the subgrade layer modulus (E_3) is 50 MPa. The increases of ε_t due to the MCP over that due to the CCP are monotonically decreasing with the increase of E_1. At E_1 = 500 MPa, the percentage increases of ε_t due to the MCP over that due to the CCP are 15.4%, 21.9%, and 32.5% for E_2 = 50, 250, and 500 MPa, respectively. At E_1 = 6000 MPa, the percentage increases are 7.2%, 8.7%, and 10.7% for E_2 = 50, 250, and 500 MPa, respectively.

Figure 11 illustrates the variations of ε_t due to the MCP and the CCP versus E_2, where the AC layer modulus (E_1) is 1000, 3000, or 6000 MPa and the subgrade layer modulus (E_3) is 50 MPa. The increases of ε_t due to the MCP over that due to the CCP are monotonically and slowly increasing with the increase of E_2. At E_2 = 50 MPa, the percentage increases of ε_t due to the MCP over that due to the CCP are 10.20%, 7.64%, and 6.54% for E_1 = 1000, 3000, and 6000 MPa, respectively. At E_2 = 1000 MPa, the percentage increases are 36.32%, 18.96%, and 13.75% for E_1 = 1000, 3000, and 6000 MPa, respectively.

Figure 12 illustrates the variations of ε_t due to the MCP and the CCP versus E_3, where the AC layer modulus (E_1) is 1000, 3000, or 6000 MPa and the base layer modulus (E_2) is 250 MPa. The increases of ε_t due to the MCP over that

Fig. 11. Maximum tensile strain at bottom of AC layer vs. base layer modulus.

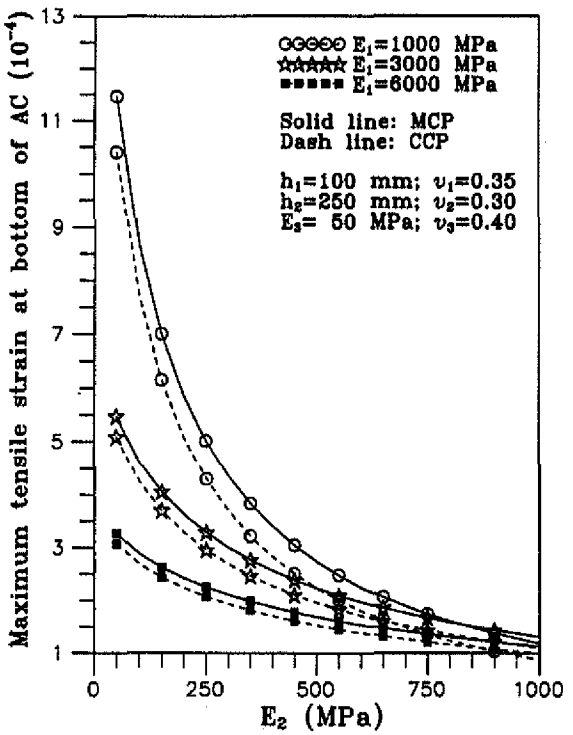

Fig. 12. Maximum tensile strain at bottom of AC layer vs. subgrade modulus.

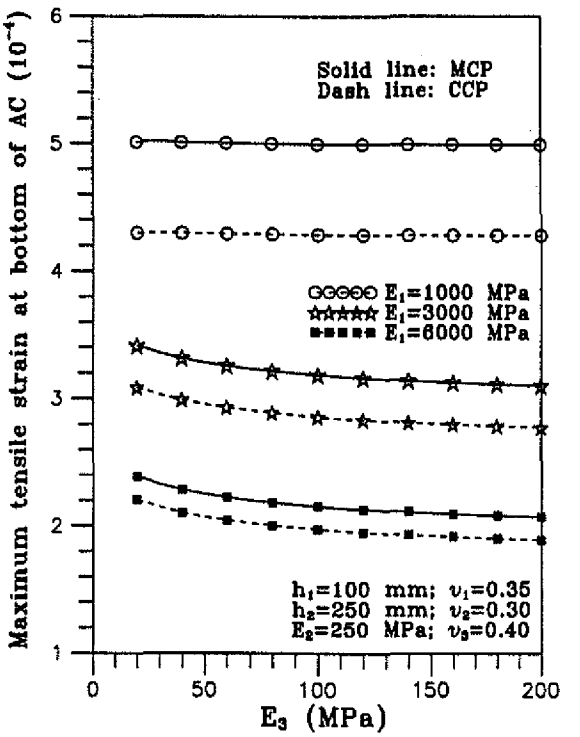

due to the CCP are very slowly increasing with the increase of E_3. At E_3 = 20 MPa, the percentage increases of ε_t due to the MCP over that due to the CCP are 16.58%, 10.53%, and 8.20% for E_1 = 1000, 3000, and 6000 MPa, respectively. At E_3 = 200 MPa, the percentage increases are 16.60%, 11.70%, and 9.57% for E_1 = 1000, 3000, and 6000 MPa, respectively.

The second sensitivity analysis example is the responses of four-layer pavement systems subjected to the actions of the two contact pressure distributions (MCP and CCP). The results are illustrated in Table 5, where six four-layer pavement systems are considered (Huang 1993). The standard case consists of an AC surface layer, a crushed stone base, a granular subbase, and a subgrade. The pavement parameters are assigned as follows: E_1 = 3500, E_2 = 200, E_3 = 100, E_4 = 30 MPa; ν_1 = 0.3, ν_2 = 0.35, ν_3 = 0.35, ν_4 = 0.45; and h_1 = 100, h_2 = 200, h_3 = 200 mm, and h_4 = ∞. The other five cases of pavement systems are formulated in such a way so that each case has only one parameter different from the standard case. Case 1 has a strong subgrade with an effective elastic modulus three times greater than that of the standard case, i.e., E_4 = 90 MPa. In case 2, all layers are assumed incompressible, i.e., $\nu_1 = \nu_2 = \nu_3 = \nu_4$ = 0.5. The granular base is replaced by an asphalt base with E_2 = 2000 MPa in case 3 and by a cement-treated base with E_2 = 6000 MPa in case 4. In case 5, a five-layer system is used with the top 350 mm of the subgrade of the standard case replaced by a lime-stabilized layer with E_4 = 150 MPa and ν_4 = 0.45.

The comparisons of effects due to the MCP and the CCP are focused on the pavement responses at the surface and interfaces. The variables of the pavement responses include (*i*) the maximum surface deflection, w_0; (*ii*) the maximum tensile strain ε_t at the bottom of the AC layer; (*iii*) the maximum vertical normal stress σ_z at each interface; (*iv*) the maximum radial normal stresses σ_r at the top and bottom of each layer; and (*v*) the maximum vertical compressive strain ε_c at the top of the subgrade. The following observations can be made from the digital results in Table 5.

(a) The values of w_0 due to the MCP are slightly larger than those due to the CCP for all the six cases (less than 1.5%).

(b) The values of ε_t and σ_r at the bottom of the AC layer due to the MCP are more than 7% higher than those due to the CCP for all the cases except case 4. In case 4, the values of ε_t and σ_r at the bottom of the AC layer due to the CCP are negative, which indicates that the bottom of the AC layer is not in tension horizontally under the action of the CCP. Besides, although ε_t at the bottom of the AC layer due to the MCP is positive, it is very small (0.031×10^{-4}); and σ_r is negative (= -0.027).

(c) For all six cases, the values of σ_z at the interface between AC and base layers due to the MCP are more than 4.6% higher than those due to the CCP.

(d) At the interfaces between the base and subbase layers, the increases of σ_z and σ_r due to the MCP over those due to the CCP are very small.

(e) At the interfaces between the subbase and subgrade layers, there are almost no differences in the values of σ_z and σ_r due to the MCP and the CCP. In particular, the values of ε_c due to the MCP are less than 0.5% higher than those due to the CCP.

7. Conclusions and recommendations

The paper presents the theoretical background for the development of a computer program VIEM using a discretization technique. Numerical verification presented in the paper

Table 5. Sensitivity analysis of pavement responses due to two contact pressure distributions (MCP and CCP).

Location	Response	Cases of pavement systems					
		Standard	1	2	3	4	5
Top of AC	w_0 (mm)	0.736	0.456	0.722	0.457	0.374	0.623
		(0.729)	(0.449)	(0.716)	(0.452)	(0.369)	(0.616)
Bottom of AC	σ_r (MPa)	1.618	1.570	2.110	0.104	−0.248	1.551
		(1.485)	(1.439)	(1.961)	(0.063)	(−0.246)	(1.419)
	ε_t (10^{-4})	3.444	3.355	3.319	0.641	0.031	3.316
		(3.137)	(3.048)	(3.050)	(0.506)	(−0.027)	(3.009)
Top of base	σ_z (MPa)	−0.203	−0.208	−0.182	−0.486	−0.607	−0.209
		(−0.194)	(−0.198)	(−0.174)	(−0.442)	(−0.542)	(−0.199)
	σ_r (MPa)	−0.005	0.010	−0.051	−0.070	−0.306	−0.012
		(−0.008)	(−0.013)	(−0.052)	(−0.082)	(−0.317)	(−0.015)
Bottom of base	σ_r (MPa)	0.057	0.040	0.066	0.365	0.581	0.037
		(0.056)	(0.039)	(0.065)	(0.362)	(0.576)	(0.037)
Top of subbase	σ_z (MPa)	−0.047	−0.058	−0.045	−0.021	−0.013	−0.058
		(−0.047)	(−0.058)	(−0.045)	(−0.021)	(−0.013)	(−0.058)
	σ_r (MPa)	0.016	0.004	0.010	0.007	0.003	0.003
		(0.015)	(0.004)	(0.010)	(0.007)	(0.003)	(0.003)
Bottom of subbase	σ_r (MPa)	0.031	0.006	0.035	0.013	0.008	0.067
		(0.031)	(0.005)	(0.034)	(0.013)	(0.008)	(0.067)
Top of subgrade	σ_z (MPa)	−0.017	−0.029	−0.017	−0.009	−0.006	−0.010
		(−0.017)	(−0.029)	(−0.017)	(−0.009)	(−0.006)	(−0.010)
	σ_r (kPa)	0.110	−1.194	−1.483	−0.843	−1.280	−1.980
		(0.096)	(−1.219)	(−1.493)	(−0.849)	(−1.282)	(−1.982)
	ε_c (10^{-4})	−5.762	−3.085	−5.140	−2.692	−1.732	−2.862
		(−5.748)	(−3.075)	(−5.127)	(−2.687)	(−1.729)	(−2.857)

Note: Numbers in parentheses are due to the CCP, other numbers are due to the MCP.

indicates that VIEM can be used to accurately and efficiently calculate the elastic response of multilayered pavements due to the action of arbitrary tire−pavement contact pressure distributions. With the use of VIEM, a theoretical investigation is further performed to illustrate the effects of tire−pavement contact pressure distributions on the response of asphalt concrete pavements. An *in situ* measured tire−pavement contact pressure distribution is utilized in the investigation.

The results of this investigation confirm theoretically the general consensus that the details of the contact pressure distributions affect stresses and strains near the surface of the pavement, whereas the response in the lower layers depends mainly on the overall load. In particular, the contact pressure distributions have a significant effect on the horizontal tensile strains at the bottom of AC layer which control the fatigue failure of asphalt pavements.

The uniform and circular contact pressure distribution commonly used in pavement design and analysis may underestimate the tensile strain at the bottom of AC layer.

Finally, it is recommended that VIEM can be further applied to the analysis of instrumented pavement response under the action of actual contact pressure distributions.

Acknowledgements

The authors would like to thank the referees for their constructive comments which enhanced the presentation of this paper.

References

Bickford, W.B. 1990. A first course in finite element method. Richard D. Irwin, Inc., Boston, Mass.

Chen, H.H., Marshek, K.M., and Saraf, C.L. 1986. Effects of truck tire contact pressure distribution on the design of flexible pavements: a three-dimensional finite element approach. Transportation Research Board, National Research Council, Washington, D.C., Transportation Research Record 1095, pp. 72−78.

Christison, J.T. 1989. Pavement response/tire pressure study. Alberta Research Council, Edmonton, Alta., Report No. HTE 89/07.

Christison, J.T., Anderson, K.O., and Shields, B.P. 1978. In situ measurements of strains and deflections in a full-depth asphaltic concrete pavement. Proceedings of the Association of Asphalt Paving Technologists, Lake Buena Vista, Fla., Vol. 47, pp. 398−433.

de Beer, M. 1994. Measurement of tire/pavement interface stresses under moving wheel loads. Reprint, Third Conference on Vehicle-Road and Vehicle-Bridge Interaction, June 5−10, Noordwijkerhout, The Netherlands. Research Report DPVT 224, Pavement Engineering Technology, Division of Roads and Transport Technology, CSIR, P.O. Box 395, Pretoria 001, South Africa.

Duncan, J.M., Monismith, C.L., and Wilson, E.L. 1968. Finite element analysis of pavements. Highway Research Board, Washington, D.C., Highway Research Record 228, pp. 18−33.

Groenendijk, J., Vogelzang, C.H., Molenaar, A.A.A., and Dohmen, L.J.M. 1994. Performance tests under accelerated

loading with the LINTRACK test facility in the Netherlands. Proceedings of the Fourth International Conference on Bearing Capacity of Roads and Airfields, Minneapolis, Minn., July, pp. 1163–1179.

Huang, Y.H. 1993. Pavement analysis and design. Prentice-Hall, Englewood Cliffs, N.J.

Huhtala, M., and Pihlajamaki, J. 1990. Truck tires and pavements. Proceedings of the Third International Conference on Bearing Capacity of Roads and Airfields, Trondheim, Norway, July, pp. 669–679.

Krarup, J. 1991. Instrumentation for a full-scale pavement test in the Danish road testing machine. *In* Road and airport pavement response monitoring system. *Edited by* V.C. Janoo and R.A. Eaton. American Society of Civil Engineers, New York. pp. 96–111.

Marshek, K.M., Chen, H.H., Connell, R.B., and Hudson, W.R. 1986*a*. Experimental determination of pressure distribution of truck tire–pavement contact. Transportation Research Board, National Research Council, Washington, D.C., Transportation Research Record 1070, pp. 9–14.

Marshek, K.M., Chen, H.H., Connell, R.B., and Saraf, C.L. 1986*b*. Effect of truck tire inflation pressure and axle load on flexible and rigid pavement performance. Transportation Research Board, National Research Council, Washington, D.C., Transportation Research Record 1070, pp. 14–21.

Monismith, C.L. 1992. Analytical based asphalt pavement design and rehabilitation: theory to practice, 1962–1992. Transportation Research Board, National Research Council, Washington, D.C., Transportation Research Record 1354, pp. 5–26.

Morris, J.R. 1987. Effect of heavy vehicle characteristics on pavement responses and performance — phase I. National Cooperative Highway Research Program, Transportation Research Board, Washington, D.C., Report No. 1-25, August.

Roberts, F.L. 1987. Flexible pavement strains caused by auto tires. ASCE Journal of Transportation Engineering, **113**: 471–483.

Schiffman, R.L. 1962. General analysis of stresses and displacements in layered elastic systems. Proceeding of International Conference on the Structural Design of Asphalt Pavements. University of Michigan, Ann Arbor, Mich., August, pp. 369–384.

Sharma, K.G., and Rao, V.G. 1984. Stresses and displacements in an elastic mass due to distributed loading by discretization technique. International Journal for Numerical and Analytical Methods in Geomechanics, **8**: 427–444.

Tielking, J.T., and Roberts, F.L. 1987. Tire contact pressure and its effect on pavement strain. ASCE Journal of Transportation Engineering, **113**: 56–250.

Uzan, J., and Sides, A. 1987. The effect of contact area shape and pressure distribution on multilayer systems response. Transportation Research Board, National Research Council, Washington, D.C., Transportation Research Record 1117, pp. 21–24.

Yue, Z.Q. 1995. On elastostatics of multilayered solids subjected to general surface traction. Quarterly Journal of Mechanics and Applied Mathematics. In press.

List of symbols

a	radius of a circular contact area
A	imprint area
E_j	elastic modulus of the jth layer
$G(x, y, z)$	point load solution of a multilayer elastic solid
h_j	thickness of the jth layer
$I_k(x, y, z)$	integral over discretized triangular or quadrilateral elements A_k (k = 1, 2, ..., N)
j	positive integer (1, 2, 3, 4, 5, ...)
J_m	Bessel function of the order m (m = 0, 1, 2)
$\|J(s, t)\|$	determinant of the Jacobian matrix
m (or n)	Gauss integration number for the local coordinate s (or t)
$N_l(s, t)$	nondimensional interpolation functions of the six-node triangular (or the eight-node quadrilateral) element, (l = 1, 2, ..., 6 (or 8))
$p(x, y)$	arbitrary tire–pavement contact pressure distribution
p_l	inputted pressure values at the node point l (l = 1, 2, ..., 6 (or 8))
P_z	total tire load
r	radial coordinate of a cylindrical coordinate system
R	$\sqrt{x^2 + y^2 + z^2}$
s_i (or t_j)	Gauss point
$S(r, z)$	axisymmetrical solution of a pavement subject to a uniform circular contact pressure
$S(x, y, z)$	solution of a multilayer elastic pavement subject to surface traction
w_0	maximum surface deflection
w_i	Gauss weight
x	independent variable of the x-axis in a Cartesian coordinate system
y	independent variable of the y-axis in a Cartesian coordinate system
z	independent variable of the z-axis in a Cartesian or cylindrical coordinate system
ε_c	maximum compressive strain at the top of subgrade
ε_t	maximum tensile strain at the bottom of asphalt concrete layer
ε_{tmax}	maximum horizontal tensile strains in the pavement
Φ	analytical kernel functions of a multilayer elastic system
ξ_l (or η_l)	node coordinate in the global coordinate system
ν_j	Poisson ratio of the jth layer
σ_r	maximum radial normal stresses at the top and bottom of each structural layer
σ_z	maximum vertical normal stress at each interface